In vitro effects of an *in silico*-modelled 17β-estradiol derivative in combination with dichloroacetic acid on MCF-7 and MCF-12A cells

X. X. Stander, B. A. Stander, A. M. Joubert

Department of Physiology, University of Pretoria, Pretoria, South Africa

Correspondence: X. X. Stander, Department of Physiology, University of Pretoria, P.O. Box 2034, Pretoria 0001, Gauteng, South Africa.
Tel.: +27 12 319 2339; Fax: +27 12 321 1679;
E-mail: xiaoxing.stander@up.ac.za

Abstract:

Objectives: To investigate the antiproliferative properties of a novel *in silico*-modelled 17β-estradiol derivative (C9) in combination with dichloroacetic acid (DCA) on MCF-7 and MCF-12A cells.

Materials and methods: xCELLigence system was employed to determine the optimal seeding number. A crystal violet assay was used to assess cell numbers and to determine the IC_{50} value (24 h) for the combination treatment. Light and fluorescent microscopy techniques were used to morphologically detect types of cell death. Flow cytometry was used to analyze the cell cycle and apoptosis.

Results: The optimal seeding number for 96-well plates was determined to be 5000-10000 cells per well for MCF-7 and MCF-12A cells. The IC_{50} for MCF-7 cells of the combination treatment after 24 h is 130 nM of C9 in conjunction with 7.5 mM of DCA ($P < 0.05$). In contrast, the same concentration inhibited cell growth by only 29.3% in the MCF-12A cells after 24 h treatment ($P < 0.05$). Morphological studies revealed decreased cell density in both types of combination-treated cells. Flow cytometric analyses demonstrated an increase in the sub-G_1 phase in combination-treated MCF-7 cells.

Conclusions: These results demonstrate that the novel 17β-estradiol derivative C9 in combination with DCA is a potent antiproliferative treatment with properties of selectivity towards tumorigenic cells and warrants further studies as a potential combination chemotherapeutic agent in other cancer cell lines.

Introduction:

The mitotic spindle, which is composed of long and hollow structures of microtubules, is intimately involved in mitosis and cell division (1,2). Naturally occurring chemical compounds such as paclitaxel, vinca alkaloids, colchicine alkaloids, as well as 2-methoxyestradiol (2ME) that target microtubules and inhibit the normal function of the mitotic spindle are one of the most researched classes of cancer chemotherapeutic drugs (1-5). 2ME (Figure 1A) is produced in trace amounts in the human body and is an endogenous metabolite derivative of estrogenic hormone 17β-estradiol with well documented antimitotic, antiangiogenic, and pro-apoptotic properties *in vitro* (6-9). 2ME abrogates microtubule

dynamics by binding to the colchicine binding site of β-tubulin (2,6,10,11). It is currently in phase I and II clinical trials for the treatment of multiple myeloma, glioblastoma multiforme and other solid tumours, such as carcinoid, prostate and breast tumours (6,12,13). However, this compound shows characteristics of low oral bioavailability that is likely caused by an additional degradation step by oxidation at the C3/C17 hydroxyl groups (14,15). Previous studies by Liu *et al.* (2005) and Newman *et al.* (2006) have emphasized the limitations of 2ME due to its potential for inactivation at the D-ring, C17 position (15,16). Panzem® NCD (NanoCrystal Dispersion), patented by Entremed, Inc. (Rockville, MD), is a nanotechnological enhanced particle of 2ME for improved dissolution (13,14,17). Zhou *et al.* (2010) mentioned that Panzem® NCD was proven to be well tolerated in cancer patients, but the anti-tumorigenic activity was modest even with heavily pre-treated (1000 mg orally four times daily) cancer patients (18,19). Therefore, 2ME analogs are under extensive research among scientists. Sulphamoylated analogs of 2ME are estrogen sulphamates that are much more potent than that of their parent estrogens (20-22). Newman *et al.* (2007) demonstrated for the first time that cyanomethyl group at C17 position significantly increased the efficacy of compounds STX640 and STX641*in vitro* and *in vivo* (23). Subsequently, Foster *et al.* (2008) demonstrated that 2-MEOe2*bis*MATE (STX140) and 2-EtE2*bis*MATE (STX 243), which are compounds exhibiting A-ring (C3 and/or C2) and D-ring (C17) modifications of 2ME, have potent anti-proliferative and anti-angiogenic activity *in vitro*, *in vivo* and *ex vivo* (24-26). The same group also showed the efficacy of STX243 against the growth of both estrogen receptor ER+ and ER- breast cancer tumours *in vitro* and *in vivo* with promising pharmacokinetic properties (25). These estrogen sulphamates are proven to obtain a higher bioavailability since they are able to overcome the biotransformation encountered by liver metabolism due to the fact that they are capable of reversibly conjugating to cytosolic erythrocyte carbonic anhydrase II (CAII) (20,21,27,28).

Carbonic anhydrases are a family of ubiquitously expressed, zinc containing isozymes that catalyze the interconversion between CO_2 and HCO_3^- (28,29). It is evidenced that the overexpression of carbonic anhydrases IX (CAIX) and XII (CAXII) is strongly associated with hypoxia, a condition favoured by most solid tumours. For example, the promoter of the CAIX gene, which contains a hypoxia response element (HRE), binds to hypoxia-inducible factor (HIF-α) in response to increased cell density and hypoxia microenvironment and activate the transcription of CAIX (21,30). The increased formation of carbonic acid as a result of CAIX expression facilitates in forming an acidotic environment surrounding solid

tumours acidosis and is known to enhance pathologic processes favoured by tumortigenicity (22,28,29). Prospective inhibitors capable of selective inhibition of hypoxia-activated CAIX therefore provide therapeutic promise for the treatment of metastatic tumours.

Several promising sulphamoylated analogs of 2ME were designed in our laboratory and 2-ethyl-3-O-sulphamoyl-estra-1,3,5(10),15-tetraen-3-ol-17-one (C9) (Figure 1B) is one of the *in silico* modelled, commercially unavailable estradiol derivatives (21). *In silico* docking performed by Stander *et al.* (2011) revealed that the 2-ethyl derivatives displayed increased binding affinity to the Colchicine-binding site when compared to other C2-modified analogs (21). This finding is in agreement with the results from another group Leese *et al.* earlier where it was discovered that an ethyl substitution at C2 position of estrone provided the optimal substituent for high anti-proliferative activity (27,31). Therefore, based on the docking results of the analogs into the colchicine site and the CAIX/CAII ratio of the compounds, it was decided to synthesize C9. Furthermore, pilot *in vitro* cell growth experiments conducted demonstrated that the mode of action of C9, similarly to its mother molecule 2ME, is attributed to its ability to disrupt mitotic spindle dynamics especially the microtubule structure, which in turn leads to a G_2/M arrest in actively diving cells regardless of the estrogen receptor status.

Not only the carbonic anhydrases pathway contributed to the acidosis. Cytosolic glycolysis also contributed to the acidotic environment as a result of the production and accumulation of lactic acid (30,32). Glucose oxidation in the mitochondria is controlled by a gate-keeping mitochondria enzyme namely pyruvate dehydrogenase (PDH). Pyruvate dehydrogenase kinase (PDK) is able to phosphorylate PDH and to inhibit the function of PDH. Dichloroacetic acid (DCA) is a well-characterized inhibitor of PDK (33). Recent studies suggest that inhibitors of PDKs attenuate inhibition of PDH activity therefore forcing cells into oxidative phosphorylation and suppress cancer growth (34-36). Xiao *et al.* (2010) used up to 40 mM DCA for the treatment of A549, HeLa, HCT116, and PLC cell lines *in vitro* and significant decrease in cell growth was demonstrated in all of these cell lines (37).

Liu *et al.* (2001) have proposed combination treatment of a glycolysis inhibitor in conjunction with a chemotherapeutic agent will open new windows for anticancer therapy (38). A recent study from Tagg *et al.* (2008) exhibited the glycolytic inhibitor 2-deoxy-D-glucose in combination with STX140 significantly reduced tumour volume by 76% ($P <$

0.001) *in vivo* compared to 46% ($P < 0.05$) STX140 only treated xenograft models (39). However, there is currently no literature available for the combination of both C9 and DCA for the treatment of cancer *in vitro*. The effects of C9 and DCA on tumorigenic and non-tumorigenic cell lines remain to be elucidated. Both C9 and DCA are regarded as potential anti-tumorigenic therapeutics with different targets and modes of action. It is of vital importance to examine and compare the effects of these compounds by investigating the *in vitro* effects on carcinogenic cells and non-carcinogenic cells. Thus, the aim of this study was to evaluate the *in vitro* influence of C9 in combination with DCA on cell growth, morphology, cell cycle progression and cell death in tumorigenic adenocarcinoma MCF-7 and non-tumorigenic MCF-12A breast epithelial cell lines.

Materials and Methods:

Cell lines

The MCF-7 cell line (estrogen receptor positive) is derived from a pleural effusion of human breast adenocarcinoma provided by Highveld Biological Pty (Ltd). (Sandringham, Johannesburg, SA). The MCF-12A cell line (estrogen receptor negative) is a non-tumorigenic spontaneously immortalized adherent human breast epithelial cell line, produced by long-term culture and forms domes in confluence, established from tissue taken at reduction mammoplasty from a nulliparous patient with fibrocystic breast disease that contained focal areas of intraductal hyperplasia. The latter was obtained as a gift from Prof MI Parker (Department of Cancer Biology of the University of Cape Town, Cape Town, SA).

Reagents

Dulbecco's minimum essential eagle medium (DMEM), Ham's F12 medium, Trypsin-EDTA, crystal violet and Bouin's fixative were supplied by Sigma Chemical Co. (St. Louis, MO, USA). Heat-inactivated fetal bovine serum (FBS) (PAA Laboratories (Pty) Ltd. Morningside, QLD, Australia), sterile cell culture flasks and plates (96-well plates and 6-well plates) were obtained through Separations (Pty) Ltd. (Randburg, Johannesburg, SA). Phosphate buffered saline (PBS) was purchased from Gibco® BRL (Invitrogen, Carlsbad, California, USA). Penicillin, streptomycin and fungizone were purchased from Highveld Biological (Pty) Ltd.

(Sandringham, Johannesburg, SA). Glutaraldehyde, triton X-100, ethanol, were purchased from Merck (Munich, Germany). The demo xCELLigence system, which include the RTCA SP Station, RTCA Analyzer and RTCA Control Unit developed by ACEA Biosciences, Inc. (San Diego, CA, USA), was kindly provided by Roche Products (Pty) Ltd. (Randburg, Johannesburg, SA) and the E-plate 96 microtiter plates were purchased from Roche Products (Pty) Ltd. (Randburg, Johannesburg, SA). The Annexin V-FITC Kit was purchased from BIOCOM biotech (Pty) Ltd. (Clubview, Pretoria, SA) and manufactured by MACS Miltenyi Biotech, GmbH, Germany. All other chemicals were of analytical grade and were purchased from Sigma Chemical Co. (St. Louis, MO, USA), Southern Cross Biotechnology (Pty) Ltd. (Cape Town, SA) and Amersham Biosciences (Pittsburgh, PA, USA).

Chemical compounds and composition of appropriate controls

Compound 2-ethyl-3-O-sulphamoyl-estra-1,3,5(10),15-tetraen-3-ol-17-one (C9) was synthesized by iThemba Pharmaceuticals (Pty) Ltd (Modderfontein, Midrand, SA). DCA (powder) was purchased from Sigma Chemical Co. (St. Louis, MO, USA). A stock solution of 0.75 μM of C9 in DMSO was prepared for all subsequent experiments. The stock solution was diluted with growth medium to the required final concentrations prior to exposure. Several controls were incorporated. Firstly, cells grown under normal conditions propagated in growth medium only. Secondly, in order to determine whether the vehicle dimethyl sulphoxide (DMSO) had an effect on proliferating cells, vehicle-treated controls were included and the final DMSO concentration used to expose cells never exceeded 0.1% (v/v). Thirdly, in order to observe the differences between combination/dual treatment of 130 nM of C9 in conjunction with 7.5 mM of DCA and individual treatment of C9 (130 nM) or DCA (7.5 mM), the cells exposed with either C9 (130 nM) or DCA (7.5 mM) were included as single treatment control. Lastly, cells were treated with actinomycin D (0.2 μg/ml) to induce apoptosis and the latter served as a positive control for the induction of apoptosis.

Cell Culture

MCF-7 breast adenocarcinoma tumorigenic cells were cultured in DMEM and supplemented with 10% heat-inactivated FBS, 1% penicillin G (100 U/ml), streptomycin (100 μg/ml) and fungizone (250 μg/l). MCF-12A non-tumorigenic breast epithelial cells were cultured in a 1:1 mixture of DMEM and Ham's F12 medium completed with epidermal growth factor (20

ng/ml), cholera toxin (100 ng/ml), insulin (0.01 mg/ml), hydrocortisone (500 ng/ml), 10% heat-inactivated FCS, 1% penicillin G (100 U/ml), streptomycin (100 µg/ml) and fungizone (250 µg/l). All cells were grown at 37°C in a humidified atmosphere containing 5% CO_2 in air.

Experiments were conducted either in 25 cm^2 culture flasks, 96-well plates or 6-well plates. For 25 cm^2 culture flasks, exponentially growing cells were seeded at 500 000 cells per 3 ml maintenance medium per flask. For six-well plates, exponentially growing cells were seeded at 375 000 cells per well in 3 ml maintenance medium on heat-sterilized cover slips. For 96-well plates, exponentially growing cells were seeded at 5000 cells per well per volume of 200 µl of maintenance medium. For E-Plate 96 microtiter plate, exponentially growing cells were seeded at densities of 20 000, 10 000, 5 000, 2 500 per well per 200 µl of medium for the proliferation assays and subsequently seeded at 10 000 per well per 200 µl of medium for cytotoxicity assays (as suggested by supplier's manual). Cells used in all experiments were allowed for a 24 h incubation period for cell adherence and medium were renewed prior to exposure.

CELL QUALITY ASSESSMENT

Real-time cell proliferation assays

The xCELLigence System (Real-Time Cell Analyzer Single Plate (RTCA SP®) system) was developed by ACEA Biosciences, Inc. (San Diego, CA, USA) in conjunction with Roche Diagnostics GmbH (Roche Applied Science, 68298 Mannheim, Germany) to monitor cellular events in real time without incorporation of dyes by measuring electrical impedance created by cells (40,41). The RTCA SP Station was connected to the RTCA Analyzer and subsequently joined the RTCA Control Unit. The xCELLigence System was connected and tested via Resistor Plate Verification before the RTCA SP Station was placed inside the incubator at 37°C and 5% CO_2. Cells were seeded at four different densities which were 20 000, 10 000, 5 000 and 2 500 cells per well in E-Plate 96 microtiter plate devices (E-Plate™, as suggested by supplier's manual). Briefly, cells were trypsinized, counted using the trypan blue exclusion method via hemacytometer and resuspended in growth medium. Background measurements were taken by adding 100 µl of the appropriate medium to the wells of the E-Plate 96. Subsequently RTCA Software Package 1.2 was used to calibrate the plates. Cells

were trypsinized and prepared into a 400 000 cell/ml stock solution prior to exposure. A volume of 100 µl of the cell suspension was added to the wells of the E-Plate 96 which contained the 100 µl of growth medium which made the final volume equal to 200 µl. MCF-7 and MCF-12A at densities of 20 000, 10 000, 5 000 and 2 500 cells per well were seeded and allowed to settle down at the bottom of the well at room temperature for 30 minutes before placing the E-Plate 96 onto the RTCA SP Station. Cell attachment and proliferation were continuously monitored for a period of 48 h as indicated using the RTCA Control Unit. While the seeded cells were propagated inside the incubator, the impedance values were converted into a cell index (CI) value corresponding to each well. The CI value is defined as the relative change in measured electrical impedance to represent cell status and it is directly proportional to the quantity, size, and attachment forces of the cell.

CELL NUMBERS

Crystal violet assay

In order to determine the growth inhibitory effect of the dual treatment on both cell lines as well, as the optimal exposure conditions, various time- (24 h, 48 h and 72h) and dose- (C9: 100 nM - 200 nM; DCA: 2.5 mM - 40 mM) dependent cell proliferation studies were conducted prior to final combination of dosage selection. Dosages chosen for C9 were based on previous in vitro cell proliferation assays conducted in our laboratory (data not shown) and the concentrations selected for DCA were supported by literature (37,42,43). Quantification of fixated monolayer cells was spectrophotometrically determined by employing crystal violet as a DNA stain. Staining cell nuclei of fixed cells with crystal violet allows for rapid, accurate and reproducible quantification of cell number in cultures grown in 96-well plates (44,45). The growth inhibitory effect (IC_{50}) was calculated as described by the National Cancer Institute (NCI, USA) in order to compare the growth inhibition induced by the compounds on the various cell lines (46).

MORPHOLOGICAL STUDIES

Optical transmitted light differential interference contrast

Polarization-optical differential interference contrast (PlasDIC) is a polarization-optical transmitted light differential interference contrast method from Zeiss (Carl Zeiss MicroImaging GmbH, Göttingen, Germany). Unlike the traditional DIC method (Smith/Nomarski DIC method), the improved PlasDIC equipment positioned the polarizer and Wollaston prism after the light has already passed through the object and objective to create image quality of excellencies (47,48). PlasDIC contrast system allows the use of plastic dishes for microscopic examinations and deliver quality optical imaging, in particular, assessment of thick cells that lie in close proximity or form groups. Images of living cells were captured before and after the appropriate exposure in order to gain insight into the effects of the newly synthesized compounds on cellular morphological changes.

Fluorescent microscopy

Fluorescent microscopy was employed to differentiate between viable, apoptotic, autophagic and oncotic cells. A triple fluorescent dye staining method was developed utilizing acridine orange (green), Hoechst 33342 (blue) and propidium iodide (red) fluorescent dyes. Acridine orange is a lysosomotropic fluorescent compound that serves as a tracer for acidic vesicular organelles including autophagic vacuoles and lysosomes (49). Hoechst 33342 is a fluorescent dye that penetrates intact cell membranes of viable cells and cells that are undergoing apoptosis and stain their nucleus. Propidium iodide (PI) is a fluorescent dye that is unable to penetrate an intact membrane and therefore stains the nucleus of cells that have lost their membrane's integrity due to oncotic and/or necrotic processes.

Exponentially growing MCF-7 and MCF-12A cells were seeded at 375 000 cells per well in six-well plates. After 24 h recovery and attachment, cells were exposed to treatments. After a 24 h exposure period, 500 µl of Hoechst 33342 solution (3.5 µg/ml) was added to the medium to obtain a final concentration of 0.9 µM and the plates were incubated for 25 minutes. Subsequently, 500 µl of acridine orange solution (4 µg/ml), as well as 500 µl propidium iodide solution (40 µg/ml) were added simultaneously to provide a final concentration of 1 µg/ml and 12 µM respectively. The plates were incubated further for five more minutes. In order to prevent fluorescent dye quenching, all procedures were performed in a dark room. Cells were examined with a Zeiss inverted Axiovert CFL40 microscope and Zeiss Axiovert MRm monochrome camera (Carl Zeiss MicroImaging GmbH, Göttingen, Germany) under

Zeiss filter 2, 9 and 15 for Hoechst 33342- (blue), acridine orange- (green) and propidium iodide-stained cells respectively.

CELL CYCLE ANALYSIS

Flow cytometry was utilized to analyze the effects of C9 and DCA on cell cycle progression of MCF-7 and MCF-12A cells. Propidium iodide was used to stain the nucleus in order to determine the amount of DNA present. The latter correlates with stages of the cell cycle during cell division. Propidium iodide fluorescence (relative DNA content per cell) was measured with a fluorescence activated cell sorting (FACS) FC500 System flow cytometer (Beckman Coulter SA (Pty) Ltd.) equipped with an air-cooled argon laser excited at 488 nm. Data from at least 10 000 cells per sample were analyzed with CXP software (Beckman Coulter SA (Pty) Ltd). Data from cell debris (particles smaller than apoptotic bodies) and clumps of two or more cells were removed to display more accurate data. Cell cycle distributions were calculated with non-commercialized Cyflogic software 1.2.1 (Pertu Therho, Turku, Finland) by assigning relative DNA content per cell to sub-G_1, G_1, S and G_2/M fractions. Propidium iodide molecules emit light at 617 nm, therefore, data obtained from the log forward scatter detector nr 3 (Fl3 log, detects 600 nm emissions) was represented as histograms on the x-axis.

Exponentially growing MCF-7 and MCF-12A cells were seeded at 500 000 cells per 25 cm^2 flask. After 24 h attachment the medium were discarded and the cells were exposed to compounds. After a 24 h exposure period, cells were trypsinized and resuspended in one millilitre of growth medium. Cells were centrifuged for five minutes to form a pellet and the supernatant was discarded. Thereafter, cells were resuspended in 200 µl of ice-cold PBS containing 0.1% FBS. Subsequently, four millilitres of ice-cold 70% ethanol were added in a drop wise manner and cells were stored for at least 24 h at 4ºC. Prior to the analyzing step, cells were pelleted by centrifugation at 300 × g for 5 minutes and resuspended in 1 ml of PBS containing propidium iodide (40 µg/ml) and incubated at 37ºC for 45 minutes.

CELL DEATH QUANTIFICATION

Annexin V-FITC

One of the earliest indications of apoptosis is the translocation of the membrane phospholipid phosphatidylserine (PS) from the inner to the outer leaflet of the plasma membrane (50). Once exposed to the extracellular environment, binding sites on PS become available for Annexin V which is a phospholipid binding protein with a high affinity for PS. Annexin V is conjugated to a fluorochrome, fluorescein isothiocyanate (FITC) and used for identification by flow cytometry for early stages of apoptosis. PS translocation also occurs during necrosis; therefore propidium iodide is used to distinguish between necrotic and early apoptotic cells.

Exponentially growing MCF-7 and MCF-12A cells were seeded (500 000 cells per 25 cm^2), attached and exposed. After 24 h exposure time, cells were trypsinized and resuspended in one millilitre of 1× Binding Buffer and were centrifuged at 300 × g for 10 minutes. The supernatant was removed and cells were washed and resupended in 100µl of 1× Binding Buffer. Annexin V-FITC (10 µl) was added and incubated with the cells for 15 minutes in the dark. Thereafter, cells were washed with one millilitre of 1× Binding Buffer and were centrifuged at 300 × g for 10 minutes. The supernatant was discarded and the cells were resuspended in 500 µl of 1× Binding Buffer solution. Immediately prior to analysis, 5 µl of propidium iodide (100 µg/ml) was added and mixed gently. Propidium iodide fluorescence (oncotic cells) and annexin V fluorescence (apoptotic cells) were measured with a fluorescence activated cell sorting (FACS) FC500 System flow cytometer (Beckman Coulter SA (Pty) Ltd.) equipped with an air-cooled argon laser excited at 488 nm. Data from at least 10 000 cells were analyzed with non-commercialized Cyflogic software 1.2.1 (Pertu Therho, Turku, Finland).

STATISTICS

Cell index calculations for real-time dynamic cell proliferation assay (n=3) were performed automatically by the RTCA Software Package 1.2 of the xCELLigence system. Experimental data from at least three biological repeats for crystal violet DNA staining (n=6), cell cycle analysis and Annexin V-FITC cell death quantification were statically analyzed. Data obtained from independent experiments are shown as the mean, standard deviation and where appropriate 95% confidence intervals. Each of the quantitative variables were statistically analysed for significance using the two-way analysis of variance (ANOVA) model with main factors treatment and cell type along with a term for the interaction between treatment and cell type. The sample sizes for quantitative experiments were at least three and data

presented are representative of one of the three such experiment. The student's *t*-test was applied where two groups of data were compared. Means are presented in bar charts, with T-bars referring to standard deviations. *P*-values of <0.05 were regarded as statistically significant and are indicated by an asterisk (*). Qualitative experiments were repeated at least twice where data was obtained from PlasDIC and fluorescent microscopy.

RESULTS

CELL QUALITY ASSESSMENT

Real-time cell proliferation assays

The xCELLigence System allows for real-time dynamic monitoring of cell attachment, adhesion and proliferation. Dynamic cell proliferation of MCF-7 and MCF-12A cells plated on the E-Plates 96 was monitored in 30-minute intervals from the time of plating until the end of the experiment. The E-Plates 96 mimic the ordinary 96-well microtiter plate except for the addition of the ultra thin sheath of gold underneath the plastic plate which serves as microelectrode to conduct current across the plate. The presence of cells on top of the thin sheath of gold will disturb the local current, thus introduce electrode impedance to the local ionic environment. Therefore, any types of cell morphological alteration will cause changes in impedance value and ultimately convert into a value named CI value. The latter value is directly proportional to the impedance value.

MCF-7 and MCF-12A at densities of 20 000, 10 000, 5 000 and 2 500 cells per well in E-Plates 96 were seeded and observed for a period of 48 h (Figures 2). Growth curves generated via the xCELLigence System revealed that MCF-7 and MCF-12A each have a distinctive trend of cell proliferation profile. MCF-7 displayed a rapid attachment over the first two hours followed by a relatively long lag phase depended on the number of cells seeded per well and finally entered a exponential growth phase (Figure 2A). MCF-12A cells showed a sharp increase of cell index after one hour of seeding when compared to MCF-7 cells (Figure 2B). The negative control (medium only without any cells) revealed that the medium is free from contamination (Figure 2). Therefore, the increases in impedance value of the curves other than negative control are purely from cell proliferation of MCF-7 (Figure 2A) and

MCF-12A (Figure 2B) cells. The impedance cell index of 20 000, 10 000, 5 000 and 2 500 cells per well increased proportionally to cell numbers of both MCF-7 and MCF-12A cells (Figure 3) with an exception of 20 000 cells/well for the MCF-12A cells. The cell index value of MCF-7 and MCF-12A at 20 000 cells/well was statistically significant with $P < 0.05$ (Figure 3).

It is of vital importance to ensure cell quality and correct amount of cells per specific surface area for any *in vitro* cellular experiments to avoid false positive or negative results. Proliferation curves of MCF-12A cells revealed that at the higher densities 20 000 cells/well (Figure 2B), cells reached plateau rapidly and the CI declined. This is possibly caused by contact inhibition. At a density of 20 000 cells per well, MCF-7 and MCF-12A cells stopped to proliferate at 40h and at 24 h respectively post-seeding due to contact inhibition, thus, making it unsuitable to conduct 24 h cell growth studies. In contrast, at the density of 2 500 cells per well, both cell lines did not show typical characteristics of proliferation. Furthermore, at the densities of 5000 and 10 000 cells per well, cells were actively proliferating at 24 h after seeding (Figure 3). It was demonstrated the most suited amount of cells per 0.32 cm^2, which is the surface area of a single well of 96-well plate, for this comparative studies was either 10 000 or 5 000 cells. Subsequently, 5000 cells per 0.32 cm^2 were selected for the crystal violet experiments as the cells reach confluency later than that of the 10 000 cells per well.

CELL GROWTH

Crystal violet assay

Dose- and time-dependent cell growth studies (data not shown) were conducted for the selection of optimal exposure conditions. A study conducted in our laboratory by Stander *et al.* (21) revealed the GI_{50} value for C9-exposed MCF-7 cells to be 130 nM after 48 hours of exposure. This concentration served as the benchmark for the concentration selection of the dual treatment. The selection of the concentration for combination therapy was conducted by setting up one non-variable constant (C9 with concentration of 130 nM) and combine it with a range of different concentrations of dichloroacetic acid (2.5, 5.0, 7.5, 10.0, 15.0 and 40.0 mM) The range of concentrations for DCA was based on other studies using similar concentrations (37,42). Neither 2.5 mM nor 5.0 mM of DCA in combination with 130 nM of

C9 inhibited MCF-7 cell growth by more than 30% and 40 mM DCA was too concentrated therefore not suitable for further *in vivo* usage. Amongst concentrations of 7.5 mM, 10.0 mM and 15 mM DCA, 7.5 mM DCA combined with C9 (130 nM) achieved similar inhibition effect compared to the other two concentrations combined with C9 with no statistically significant differences (data not shown). Finally, 130 nM of C9 in combination with 7.5 mM of DCA inhibited MCF-7 cell growth to about 50% after 24 h, therefore, this concentration and time point was chosen for all subsequent experiments.

Cell growth analysis by means of crystal violet DNA staining revealed that compound C9-exposed MCF-7 cells demonstrated approximately 20% cell growth inhibition compared to vehicle exposed MCF-7 cells ($P < 0.05$) after 24 h of exposure (Figure 4). DCA-exposed (24 h) MCF-7 cells did not show significant cell inhibition compared to control (Figure 4). However, MCF-7 cell numbers after 24 h of exposure to 130 nM of C9 in combination with DCA (7.5 mM) revealed a statistically significant decrease of 50.84% ($P < 0.05$) (Figure 4).24 h. Therefore, a synergistic effect of DCA in combination with C9 was observed whereby DCA serves as an adjuvant to enhance the pharmacokinetics of the microtubule disruptor, C9, in rapidly proliferating tumorigenic cells.

For the MCF-12A cells C9 also induced cell inhibition in non-tumorigenic cells and revealed approximately 28% growth inhibition compared to the vehicle-treated control ($P < 0.05$) (Figure 4). Growth inhibition for combination-exposed MCF-12A cells was approximately 29% and was not statistically significantly different from the C9-treated MCF-12A cells (Figure 4). Therefore, no synergistic effect for combination-exposed MCF-12A cells was observed (Figure 4).
MCF-12A cells responded statistically significantly differently to the combination treatment when compared to MCF-7 cells with the MCF-7 cell growth inhibited to a greater extent (50.84%) when compared to the MCF-12A-treated cells (29%) ($P < 0.05$) (Figure 4).. The vehicle (DMSO) used to dissolve C9 was biologically and molecularly inert with no toxic effect observed on the cells with (v/v) not exceeding 0.01% (data not shown).

MORPHOLOGY

Optical transmitted light differential interference contrast

PlasDIC images of both MCF-7 and MCF-12A C9-treated cells (Figure 5 (B) and (G)) showed an increase in metaphase and formation of apoptotic bodies. DCA-treated cells (Figure 5 (C) and (H)) revealed shrunken cells compared to cells grown to confluency in the vehicle-treated control (Figure 5 (A) and (F)). Cells exposed to C9 in combination with DCA (Figure 5 (D) and (I)) displayed characteristics of cells in metaphase, formation of apoptotic bodies, shrunken cells, compromised cell density and even appearance of ghost cells. Upon dual treatment of C9 with DCA, MCF-7 cells (Figure 5(D)) displayed not only severe degree of compromised cell density but also vast number of existing cells are either in metaphase, shrunken or display characteristics of cell death (apoptosis) compared to MCF-12A cells. Therefore, MCF-7 cells (Figure 5(D)) appeared more susceptible when compared to MCF-12A cells (Figure 5I) morphologically.

MORPHOLOGY

Fluorescent microscopy

The fluorescent microscopy study revealed an increase of MCF-7 cells present in metaphase after 24 h of exposure to C9 (130 nM) (Figure 6(B)). DCA-exposed (7.5 mM) MCF-7 cells showed slightly increased acridine orange staining (Figure 6(C)) when compared to the control (Figure 6(A)). However, combination treatment of C9+DCA-exposed MCF-7 displayed severe degree of compromised cell density, increased acridine orange staining and large number of existing cells in metaphase (Figure 6(D)). Furthermore, the microscopy study showed a slight increase in acridine orange staining in C9-, DCA- and C9+DCA-exposed MCF-12A cells (Figure 6(G, H, I)). The effect of C9 or combination treatment on MCF-12A cells (Figure 6(G,I)) is moderate in comparison with MCF-7 cells (Figure 6(B,D)) that were treated under the same exposure conditions. This observation is in agreement with findings from previous cell number studies where the addition of DCA enhanced the efficacy of compound C9 in tumorigenic cells.

CELL CYCLE ANALYSIS

Previous studies demonstrated that sulphamoylated derivatives of 2ME are able to induce cell cycle arrest in a number of tumorigenic cell lines *in vitro*, as well as xenograft models (21,24). In this study, the effect of C-17 modified sulphamoylated derivatives in conjunction with a

glycolysis inhibitor on cell cycle arrest were examined in the hormone-dependent MCF-7 and hormone-independent MCF-12A cell lines. In vehicle-exposed MCF-7 cells, less than 1% of the cells are in sub-G_1 and 27% are in G_2/M (Figure 7(A) and Figure 8(A)). The antimitotic agent C9-exposed (130 nM) MCF-7 cells showed slightly elevated levels of cells present in sub-G_1 (5%) ($P = 0.13$) (Figure 7(A) and Figure 8(A)). However, C9 induced tumorigenic cell cycle arrest with 36% of cell present in G_2/M phase ($P < 0.05$) when compared to the control (Figure 7(A) and Figure 8(A)). After treatment with 7.5 mM of DCA on MCF-7 cells, no significant change in cell cycle events was observed. In contrast, we have observed that when DCA was added together with the antimitotic agent C9, the efficacy of combination therapy was superior than that of C9 alone exposed MCF-7 cells, with increased sub-G_1 (19%, $P < 0.05$) and G_2/M (35%, $P < 0.05$) phases compared to control (Figure 7(A) and Figure 8(A)). Alternatively, agent C9 at 130 nM after 24 h exposure did not induce non-tumorigenic MCF-12A G_2/M (22%) cell cycle arrest compared to control (23%) (Figure 7(B) and Figure 8(B)). The combination of C9 and DCA-exposed MCF-12A showed a statistically significant increase in sub-G_1 (10%) compared to control (5%) ($P < 0.05$). No sign of elevated G_2/M with the combination treatment was observed on MCF-12A cells (Figure 7(B) and Figure 8(B)). Combination treatment of the antimitotic agent with a glycolysis inhibitor resulted in 19% of the tumorigenic cells to be present in sub-G_1. However, only 10% of non-tumorigenic cells were in sub-G_1 when given the same circumstances. These observations were statistically significant ($P < 0.05$) (Figure 8).

CELL DEATH QUANTIFICATION

Analysis of cellular apoptosis is one of the methods to understand the possible mechanisms for C9+DCA mediated cell death. Externalization of phosphatidylserine were detected with Annexin V-FITC and measured with a flow cytometer. In terms of apoptosis induction, in both types of cells, neither the antimitotic agent C9 (130 nM) nor the glycolysis inhibitor DCA (7.5 mM) alone had a significant effect compared to controls (Figure 9). However, when both cell types went under the treatment of combination therapy (C9+DCA) for 24 h,

there are 15.3% MCF-7 and 5.7% MCF-12A cells present in early apoptosis phase and the increase is statistically significant when compared to relative controls ($P < 0.05$) (Figure 9). This finding is in agreement with the previous cell cycle analysis sub-G_1 results (Figure 8). When we evaluated the apoptosis induction results between the two cell lines, it was observed that the difference between early apoptosis for MCF-7 (15.3%) and MCF-12A (5.7%) cells are statistically significant ($P < 0.05$) (Figure 9).

Discussion and Conclusion

It was hypothesized a decade ago by Liu *et al.* that a glycolysis inhibitor in combination with a conventional chemotherapeutic agent may exhibit synergistic effects. They further proposed that the chemotherapeutics would target the fast dividing tumor cells on the edges, while the glycolysis inhibitor would focus on the cells at the hypoxic centre (38). Furthermore, Tagg *et al.* (2008) recently demonstrated that the combination of sulphamoylated 2ME analog with 2-deoxy-D-glucose was a potent therapeutic agent in breast and prostate cancer *in vivo* (39). In our study, the combination of an antimitotic agent C9 with a glycolytic inhibitor DCA served as a powerful inhibitor for breast tumorigenic cell growth *in vitro*. This study not only demonstrated that the results are in accord with previous studies by Liu *et al.* (2001) and Tagg *et al.* (2008), but it also contributes toward the understanding of combination therapy.

In the present comparative study between non-tumorigenic MCF-12A epithelial cells and breast adenocarcinoma MCF-7 cells the synergistic effects of dichloroacetic acid (7.5 mM) combined with a new antimitotic compound, C9 (130 nM), on cell proliferation, cell cycle progression and apoptosis were demonstrated. Real-time dynamic monitoring of cell adhesion and proliferation via the xCELLigence system revealed that the optimal seeding number of cells for this comparative studies in a 96-well plate is between 5000 to 10 000 cells per well. Cell growth studies employing crystal violet as a DNA stain revealed that the combination treatment of DCA at a concentration of 7.5 mM and C9 at a concentration of 130 nM inhibited cell proliferation in the tumorigenic MCF-7 cells to 50.84% after 24 h of exposure (IC_{50}). The same concentration inhibited cell growth by only 29.29% in the non-tumorigenic MCF-12A cells, indicating that the non-tumorigenic MCF-12A cells are less susceptible to growth inhibition when compared to the tumorigenic MCF-7 cell line for this specific combination of DCA and C9.

Previous research has demonstrated similar results for DCA when combined with antimitotic compounds whereby normal cells show lower cytotoxity when compared to tumorigenic cells (51-53). Olszewski *et al.* (2011) demonstrated that HEK293 normal epithelial kidney cells exhibited less cytotoxity at 10 mM DCA in combination with selected platinum drugs (51). Fiebiger *et al.* (2011) demonstrated that DCA potentiates the cytotoxicity of selected platinum drugs, including satraplatin (52). Dhar and Lippard (2009) showed that mitaplatin, another platinum-based anticancer compound, in combination with DCA selectively kills cancer cells (53). The present study is the first to demonstrate the *in vitro* effects of an antimitotic compound in combination with DCA on tumorigenic and non-tumorigenic cells.

Morphological investigation via plasDIC light microscopy indicates that DCA-treated MCF-12A and MCF-7 cells showed no significant qualitative morphological differences when compared to the vehicle-treated controls. Compromised cell density was, however, observed in both cell lines treated with C9 when compared to vehicle-treated controls. Formation of apoptotic bodies and compromised cell density in MCF-7 and MCF-12A cells treated with C9+DCA were observed. However, the MCF-12A cells appeared to be less affected when compared to the MCF-7 cells. The increase in acridine orange suggests an increase in lysosomal and/or autolysosomal activity The increase in acridine orange suggests an increase in lysosomal and/or autolysosomal activity.

Cell cycle analyses revealed an increase in G_2/M phase in C9-exposed and C9+DCA-exposed MCF-7 cells. A decrease in cells present in the S-phase, as well as an increase in the amount of cells present in the sub-G_1 phase in MCF-7-treated C9+DCA cells. This observation on MCF-7 agrees with previous studies which showed similar findings on MCF-7 cells by Tagg *et al.* (2008). There was also an increase in the sub-G_1 phase in MCF-12A-treated C9+DCA cells. In comparison, the difference between sub-G_1 portion on tumorigenic and non-tumorigenic cell lines are statistically significant ($P < 0.05$). Apoptosis analyses showed that C9-treated MCF-7 and MCF-12A cells have a comparatively similar amount of cells in early apoptosis.. DCA-treated cells showed no statistically significant difference in early and late apoptotic cells when compared to the vehicle-treated control. However, when cells were treated with C9+DCA, a synergistic effect was observed whereby the MCF-7 cells present in early apoptosis increased approximately three-fold when compared to C9-treated cells. This effect was not as pronounced in the MCF-12A cells (two-fold increase), suggesting that the

synergistic effect is selective towards the tumorigenic cells. Statistical analysis between two cell lines confirmed this finding that C9+DCA-exposed MCF-7 cells exhibited significant higher percentages of cells in early apoptosis ($P < 0.05$).

The IC_{50} suggests that MCF-7 cell growth was half as much when compared to the vehicle-treated control. This does not necessarily imply that 50% of the tumorigenic cells in fact undergo cell death. The Annexin V-FITC apoptosis study, however, suggests that approximately 16% of the cells are apoptotic after 24 h exposure with C9+DCA. Thus, from the data it can be concluded that apoptosis is but one mechanism of growth inhibition. The morphological studies qualitatively confirm that apoptotic processes are present; however, they also suggest that autophagic processes (increase in acridine orange staining) might also, in part, be responsible for cell growth inhibition. Previous studies where 2ME was used for the anticancer treatment *in vitro* have demonstrated similar findings. For example, Fukui *et al.* (2008) demonstrated that 1.5-2.0 µM of 2ME inhibited cell growth in MDA-MB-435 cells after 48 h to 50% when compared to the vehicle-treated control and 1.5 µM only induced apoptosis in 18.1% of the cells (54). Also, our group has demonstrated that 2ME inhibits growth cell growth in MCF-7 cells after 48 h to 50% at 1 µM and that it induces apoptosis in 15% of the cells at the same concentration (7).

The present study demonstrates that the combination of a new antimitotic compound in conjunction with the PDK inhibitor, DCA, has the potential to selectively target tumorigenic MCF-7 cells over non-tumorigenic MCF-12A cells by inducing apoptosis. MCF-7 cells have a high glycolytic capacity and they also have a significantly more hyperpolarized mitochondrial membrane potential compared to normal cells (55,56). Inhibitors of PDKs such as DCA attenuate inhibition of pyruvate dehydrogenase (PDH) activity. The increased PDH activity shifts metabolism from glycolysis to oxidative phosphorylation, decreasing mitochondrial membrane potential hyperpolarization which in turn opens mitochondrial transition pores (56). This allows for the translocation of ROS from the mitochondrial matrix to the cytoplasm and increases ROS-signaling, as well as restoring normal metabolism (56). Restoring normal mitochondrial membrane potential in turn results in sensitizing cells to apoptotic signaling (56).

C9 is a more potent antimitotic analogue of 2ME, however it is suggested that its mechanism of action with regards to induction of apoptosis is similar to that of 2ME. In 2ME-treated

cells, cell cycle arrest leads to apoptosis via reactive oxygen species generation and the intrinsic apoptosis induction pathway as a result of an increase in mitochondrial permeabilization and cytochrome *c* leakage (7). Autophagic activity is also regulated by reactive oxygen species (57). It is proposed that the selectivity of the combination treatment is associated with the restoration of oxidative phosphorylation in MCF-7 cells which in turn contributes to reactive oxygen species formation, mitochondrial permeabilization and ultimately culminating in apoptosis and/or autophagy induction. In conclusion, the synergistic effect of a novel antimitotic compound in conjunction with DCA on tumorigenic and non-tumorigenic cells was demonstrated for the first time. This study suggests that the specific combination DCA and C9 is more harmful for tumorigenic cells than treatment with DCA or C9 alone. Further mechanistic studies are underway to further characterize the exact mechanism of action.

Acknowledgements

This research was supported by grants from the Medical Research Council of South Africa (AL343, AS536), the Cancer Association of South Africa (AS201), the National Research Foundation (NRF) (AL239), the RESCOM of University of Pretoria and the Struwig-Germeshuysen Cancer Research Trust of South Africa (AN074). The xCELLigence was conducted at Department of Physiology, University of Pretoria with the demonstration instrument kindly provided by Roche (Randburg, South Africa) and the flow cytometric analyses were performed at the Department of Pharmacology, Faculty of Health Sciences, University of Pretoria. Special thanks to Nobantu Phalatsi (application specialist) from Roche with the help of xCELLigence instrument and the data analysis.

List of Figures

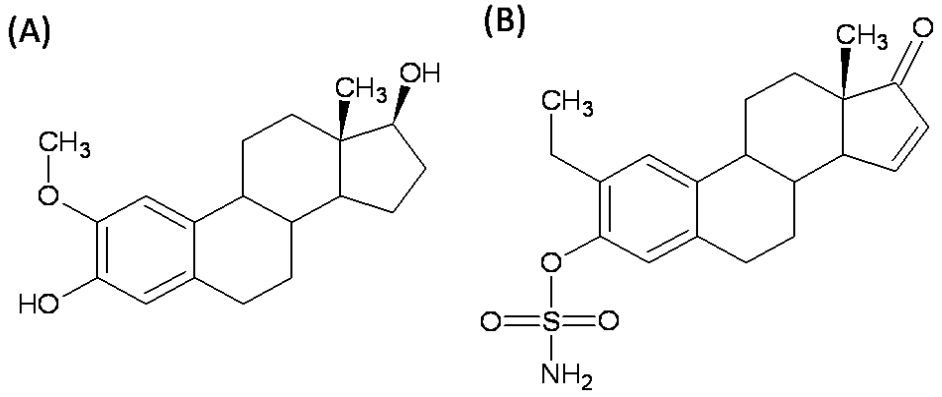

Figure 1: (A) 2-methoxyestradiol (2ME); (B) 2-ethyl-3-O-sulphamoyl-estra-1,3,5(10),15-tetraen-3-ol-17-one (C9) (ACD/ChemSketch freeware version 12.0).

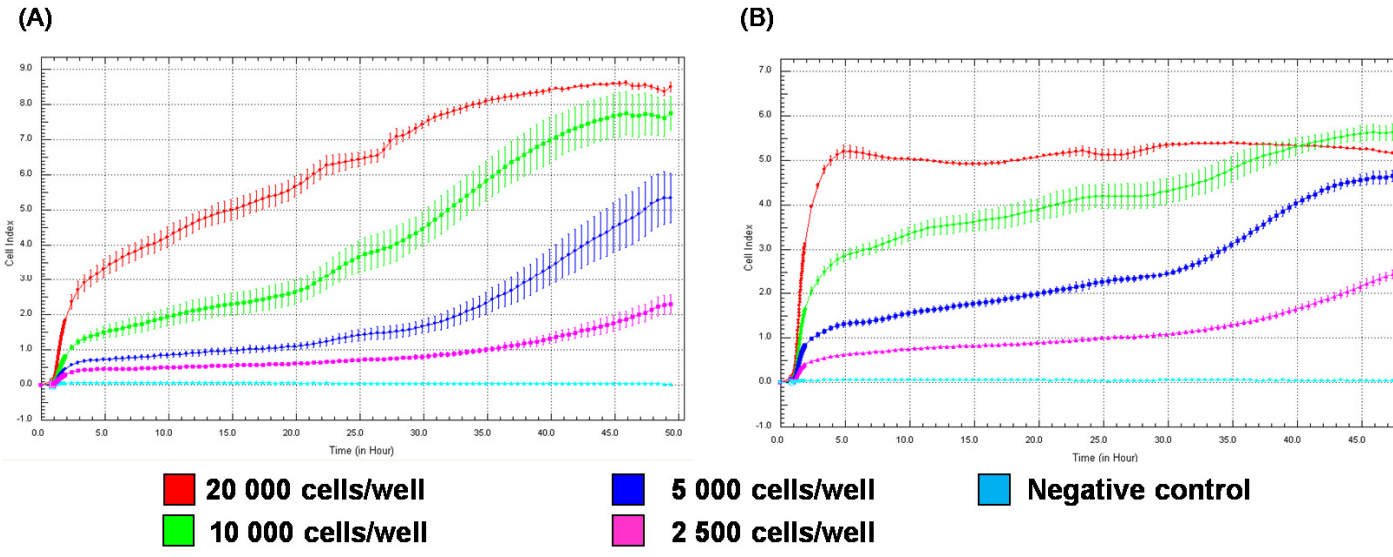

Figure 2: Real-time dynamic monitoring of cell adhesion and proliferation via the xCELLigence system. MCF-7 (A) and MCF-12A (B) seeded at densities of 20 000, 10 000, 5 000 and 2 500 cells per well in *E-Plates 96* were observed for a period of 48 h.

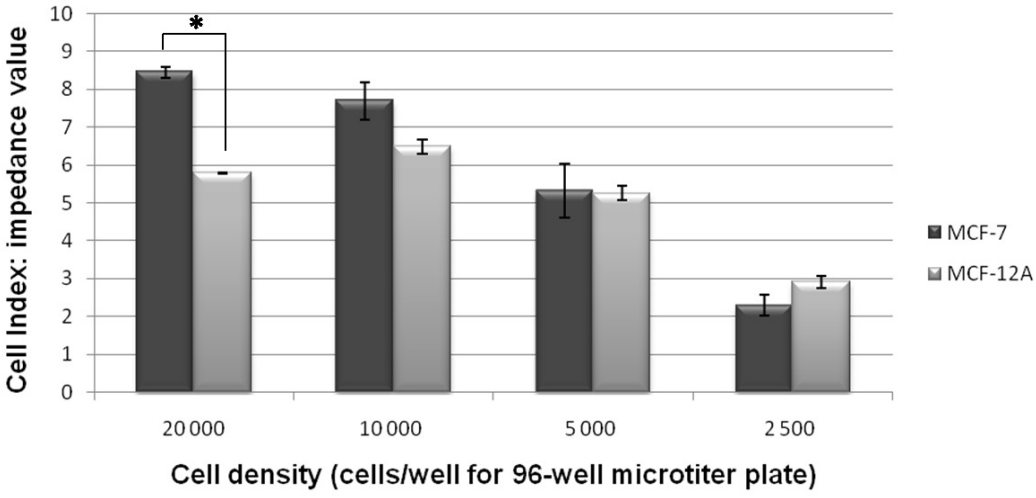

Figure 3: Cell number titration expressed as impedance value namely cell index for both MCF-7 and MCF-12A cells with cell densities of 20 000, 10 000, 5 000 and 2 500 cells/well in the E-plate 96 after being monitored for 48 h. An asterisk (*) indicates a *P*-value < 0.05 when MCF-7 and MCF-12A cells were compared.

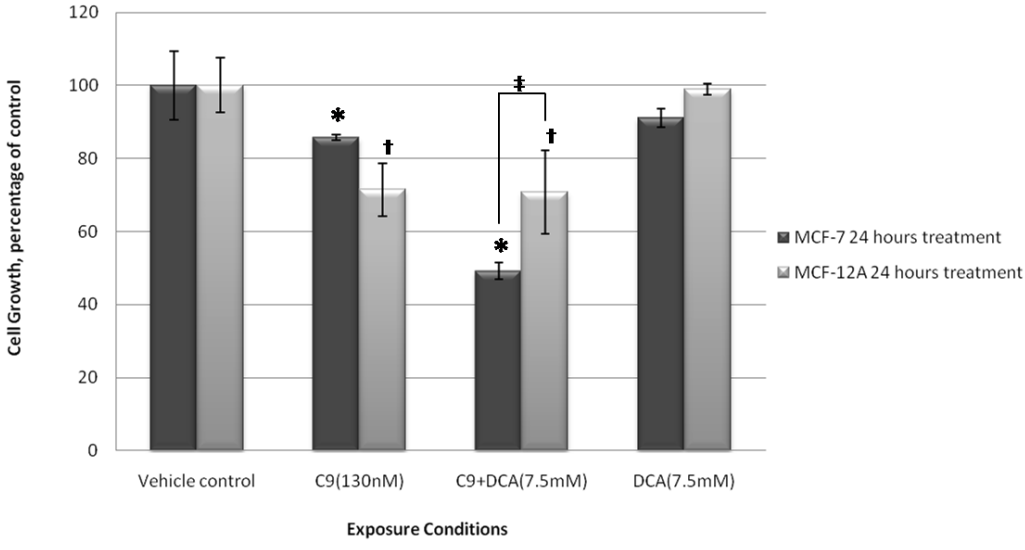

Figure 4: MCF-7 and MCF-12A cell growth expressed as a percentage of the control (cells propagated in medium and the vehicle, DMSO<0.01%) after 24 h of exposure to different conditions. An asterisk or a dagger (*, †) indicates a *P*-value < 0.05 after comparison of cells and controls within the same cell line. A double dagger (‡) indicates a *P*-value < 0.05 when MCF-7 and MCF-12A cells were compared for the same treatment.

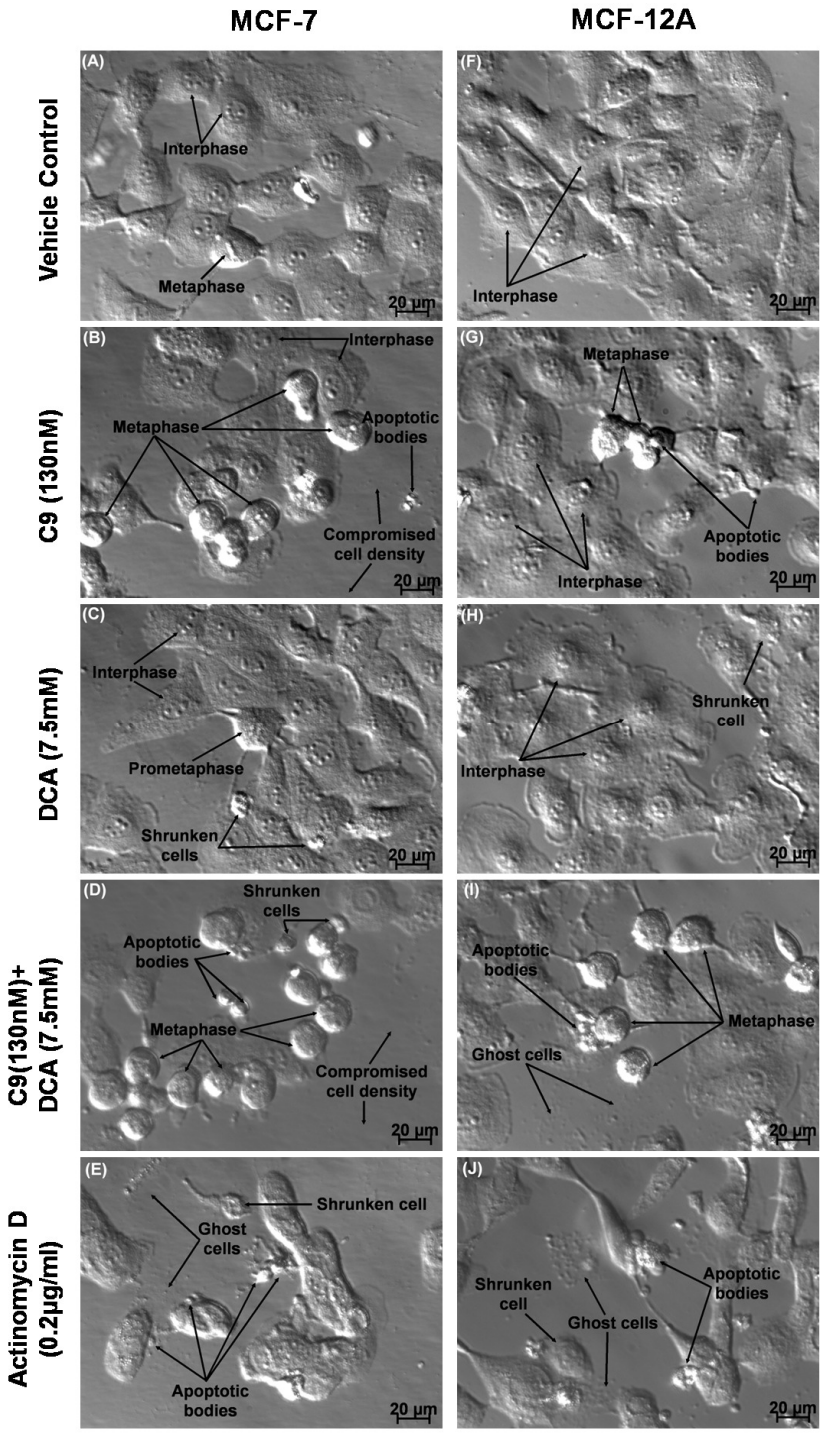

Figure 5: PlasDIC images of MCF-7 cells (left column, images A to E) compared to MCF-12A cells (right column, images F to J) after 24 h of exposure to different conditions. Vehicle-treated (A and F) cells were confluent and showed no sign of distress. C9 (130 nM) - exposed (B and G) cells showed decreased cell density and an increase in metaphase. Cells exposed to 7.5 mM of DCA (C and H) indicated no significant decrease in cell number. Cells exposed to C9 (130 nM) in combination of DCA (7.5 mM) (D and I) showed significant

inhibition of cell growth. Actinomycin D (0.2 µg/ml) -treated cells (E and J) exhibited hallmarks of late stages of apoptosis.

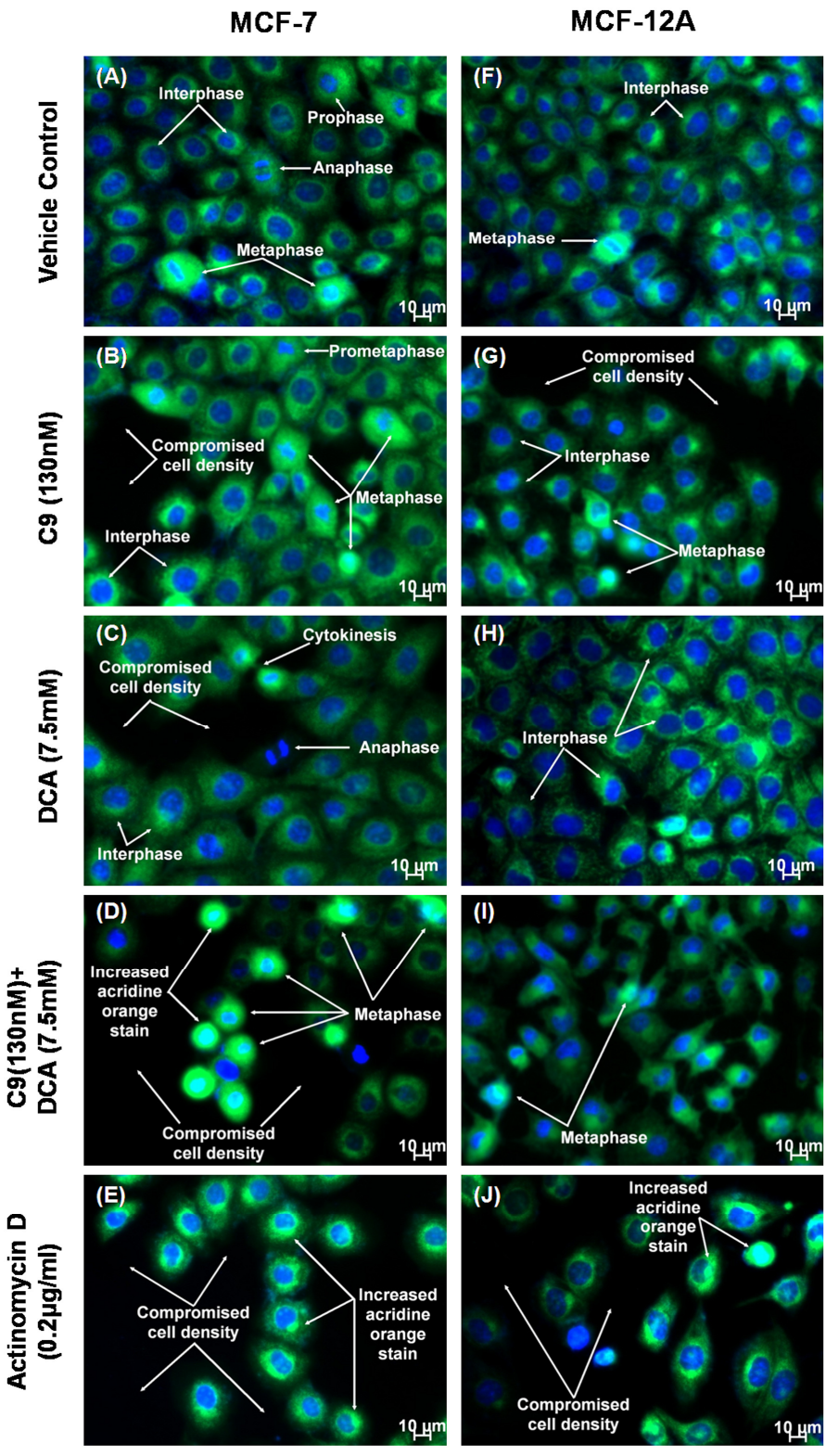

Figure 6: Fluorescent microscopy utilizing triple fluorescent stains of Hoechst 33342 (stains DNA blue), acridine orange (stains acidic vacuoles green) and propidium iodide (penetrate

cell membrane). Fluorescent images of MCF-7 cells (left column, images A to E) compared to MCF-12A cells (right column, images F to J) after 24 h of exposure to different conditions. Fluorescent images of MCF-7 cells (left column, images A to E) compared to MCF-12A cells (right column, images F to J) after 24 h of exposure to different conditions. Vehicle-treated (A and F) cells were confluent and showed no sign of distress. C9 (130 nM) -exposed (B and G) cells showed decreased cell density and an increase in metaphase. Cells exposed to 7.5 mM of DCA (C and H) indicated no significant decrease in cell number. Cells exposed to C9 (130 nM) in combination of DCA (7.5 mM) (D and I) showed significant inhibition of cell growth. Actinomycin D (0.2µg/ml) -treated cells (E and J) exhibited hallmarks of late stages of apoptosis.

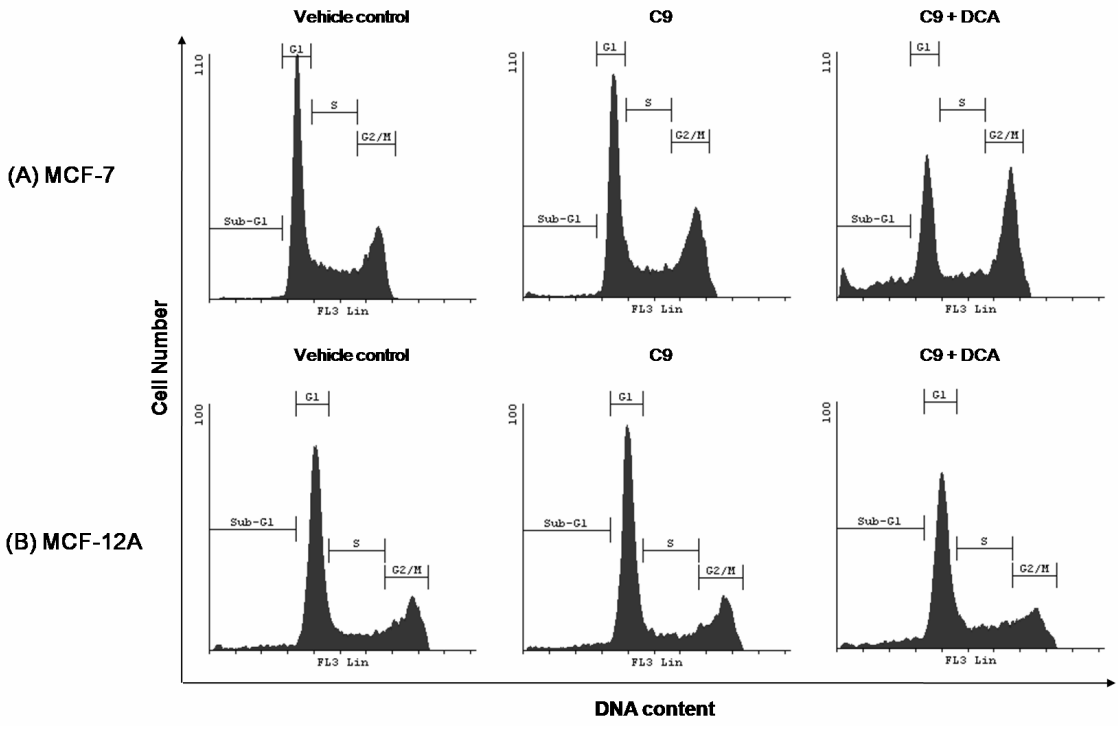

Figure 7: Cell cycle histograms of vehicle-, C9- and C9+DCA-exposed cells after 24 h treatment for (A) MCF-7 and (B) MCF-12A cells.

(A)

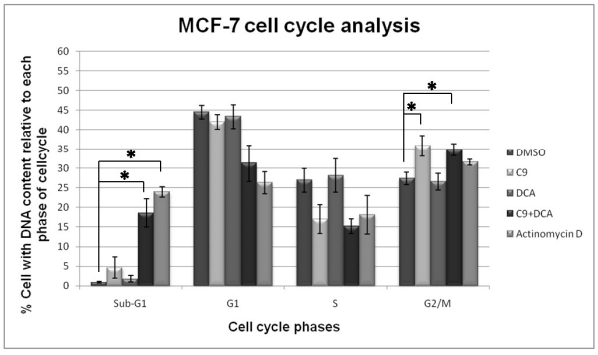

(B)

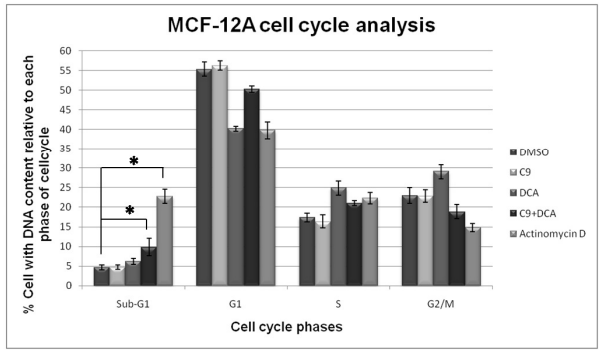

Figure 8: Distribution of DNA content relative to phase of cell cycle of both (A) MCF-7 and (B) MCF-12A cells. Data is sub-ordered to vehicle-, C9-, DCA-, C9 plus DCA- and actinomycin D (positive control for apoptosis) –exposed cells. Both cell lines indicated a statistically significant increase in the sub-G_1 phase of the C9+DCA-exposed samples compared to vehicle-treated cells. MCF-7 cells are more susceptible to the combination compounds treatment. An asterisk (*) indicates a *P*-value < 0.05 when exposed cells were compared to the vehicle controls within the same cell line.

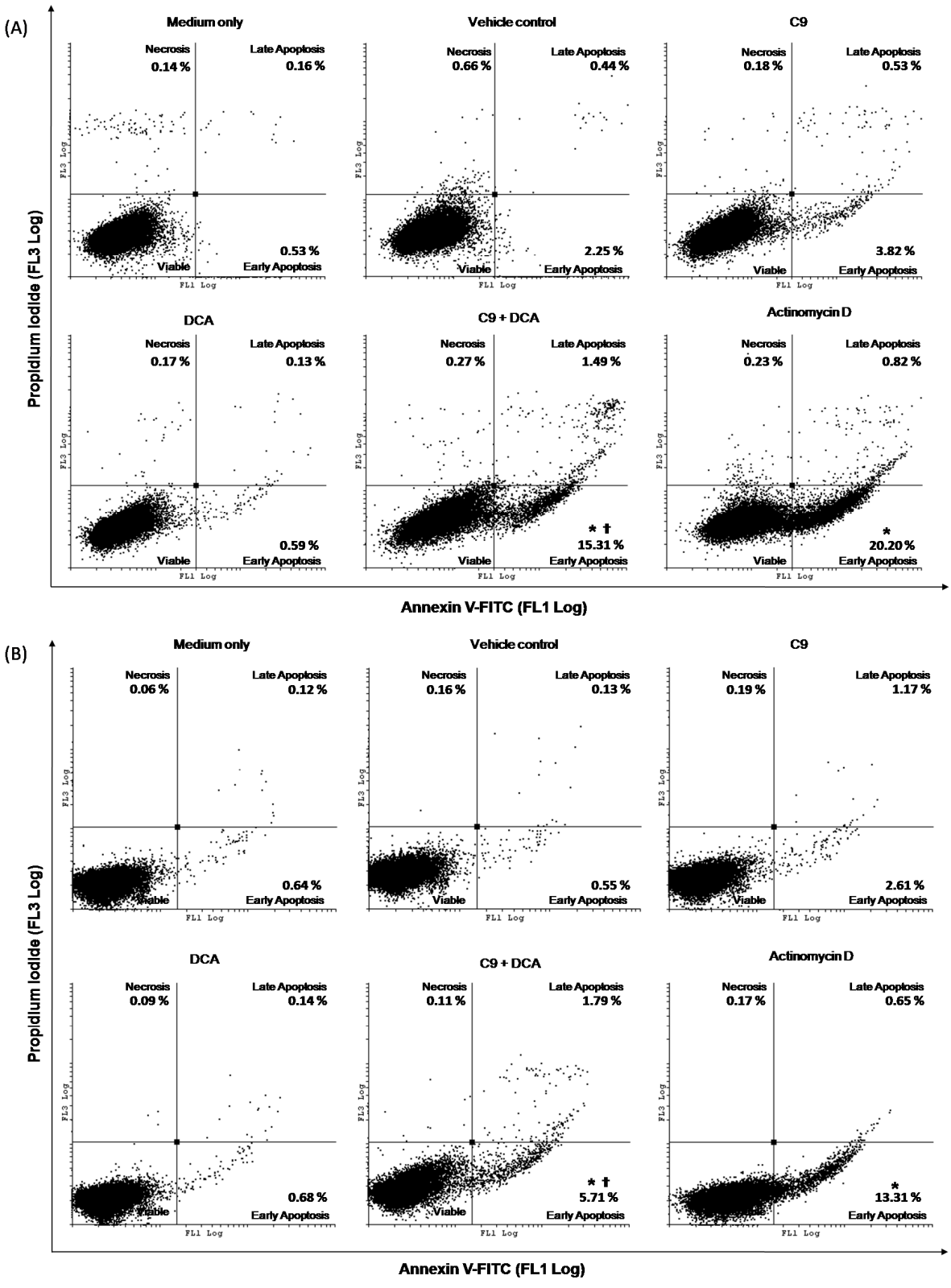

Figure 9: Apoptosis detection by means of flow cytometry and annexin V-FITC of MCF-7 (A) and MCF-12A (B) cells. Propidium iodide (FL3 Log) vs. annexin V-FITC (FL1 Log) dot-plots of cells propagated in growth medium, vehicle (DMSO)-, C9-, DCA-, C9+DCA- and actinomycin D-exposed MCF-7 (A) and MCF-12A (B) cells. Cells treated with the

vehicle control (DMSO v/v < 0.01%) revealed no toxic effect in both cell lines. Neither C9-treated nor DCA-treated MCF-7 (A) and MCF-12A (B) cells caused severe degree of apoptosis when compared to C9+DCA-exposed cells. An asterisk (*) indicates a *P*-value < 0.05 when compared to the vehicle control within the same cell line. The MCF-7 cells exposed to dual treatment induced increased early apoptosis when compared to MCF-12A cells. A dagger (†) indicates *P*-value < 0.05 when MCF-7 cells were compared to MCF-12A cells.

References

1. Zhou J, Giannakakou P. (2005) Targeting microtubules for cancer chemotherapy. *Curr Med Chem Anticancer Agents*. 5(1):65-71.
2. Islam MN, Iskander MN. (2004) Microtubulin binding sites as target for developing anticancer agents. *Mini Rev Med Chem*. 4(10):1077-1104.
3. Giannakakou P, Nakano M, Nicolaou KC, O'Brate A, Yu J, Blagosklonny MV, et al. (2002) Enhanced microtubule-dependent trafficking and p53 nuclear accumulation by suppression of microtubule dynamics. *Proc Natl Acad Sci U S A*. 99(16):10855-10860.
4. Jordan MA, Wilson L. (2004) Microtubules as a target for anticancer drugs. *Nat Rev Cancer*. 4(4):253-265.
5. Bunker JM, Wilson L, Jordan MA, Feinstein SC. (2004) Modulation of microtubule dynamics by tau in living cells: implications for development and neurodegeneration. *Mol Biol Cell*. 15(6):2720-2728.
6. Kamath K, Okouneva T, Larson G, Panda D, Wilson L, Jordan MA. (2006) 2-Methoxyestradiol suppresses microtubule dynamics and arrests mitosis without depolymerizing microtubules. *Mol Cancer Ther*. 5(9):2225-2233.
7. Stander BA, Marais S, Vorster CJ, Joubert AM. (2010) In vitro effects of 2-methoxyestradiol on morphology, cell cycle progression, cell death and gene expression changes in the tumorigenic MCF-7 breast epithelial cell line. *J Steroid Biochem Mol Biol*. 119(3-5):149-160.
8. Mueck AO, Seeger H. 2-Methoxyestradiol--biology and mechanism of action. *Steroids*. 75(10):625-631.
9. Joubert A, Marais S. (2007) In vitro effects of 2-methoxyestradiol on cell morphology and Cdc2 kinase activity in SNO oesophageal carcinoma cells. *Cell Biochem Funct*. 25(3):357-362.
10. D'Amato RJ, Lin CM, Flynn E, Folkman J, Hamel E. (1994) 2-Methoxyestradiol, an endogenous mammalian metabolite, inhibits tubulin polymerization by interacting at the colchicine site. *Proc Natl Acad Sci U S A*. 91(9):3964-3968.
11. LaVallee TM, Burke PA, Swartz GM, Hamel E, Agoston GE, Shah J, et al. (2008) Significant antitumor activity in vivo following treatment with the microtubule agent ENMD-1198. *Mol Cancer Ther*. 7(6):1472-1482.
12. Van Zijl C, Lottering ML, Steffens F, Joubert A. (2008) In vitro effects of 2-methoxyestradiol on MCF-12A and MCF-7 cell growth, morphology and mitotic spindle formation. *Cell Biochem Funct*. 26(5):632-642.
13. Vorster CJ, Joubert AM. In vitro effects of 2-methoxyestradiol-bis-sulphamate on the non-tumorigenic MCF-12A cell line. *Cell Biochem Funct*. 28(5):412-419.
14. Tevaarwerk AJ, Holen KD, Alberti DB, Sidor C, Arnott J, Quon C, et al. (2009) Phase I trial of 2-methoxyestradiol NanoCrystal dispersion in advanced solid malignancies. *Clin Cancer Res*. 15(4):1460-1465.
15. Newman SP, Ireson CR, Tutill HJ, Day JM, Parsons MF, Leese MP, et al. (2006) The role of 17beta-hydroxysteroid dehydrogenases in modulating the activity of 2-methoxyestradiol in breast cancer cells. *Cancer Res*. 66(1):324-330.
16. Liu ZJ, Lee WJ, Zhu BT. (2005) Selective insensitivity of ZR-75-1 human breast cancer cells to 2-methoxyestradiol: evidence for type II 17beta-hydroxysteroid dehydrogenase as the underlying cause. *Cancer Res*. 65(13):5802-5811.
17. James J, Murry DJ, Treston AM, Storniolo AM, Sledge GW, Sidor C, et al. (2007) Phase I safety, pharmacokinetic and pharmacodynamic studies of 2-methoxyestradiol alone or in combination with docetaxel in patients with locally recurrent or metastatic breast cancer. *Invest New Drugs*. 25(1):41-48.

18. Zhou Q, Gustafson D, Nallapareddy S, Diab S, Leong S, Lewis K, et al. (2010) A phase I dose-escalation, safety and pharmacokinetic study of the 2-methoxyestradiol analog ENMD-1198 administered orally to patients with advanced cancer. *Invest New Drugs*.
19. Matei D, Schilder J, Sutton G, Perkins S, Breen T, Quon C, et al. (2009) Activity of 2 methoxyestradiol (Panzem NCD) in advanced, platinum-resistant ovarian cancer and primary peritoneal carcinomatosis: a Hoosier Oncology Group trial. *Gynecol Oncol*. 115(1):90-96.
20. Elger W, Schwarz S, Hedden A, Reddersen G, Schneider B. (1995) Sulfamates of various estrogens are prodrugs with increased systemic and reduced hepatic estrogenicity at oral application. *J Steroid Biochem Mol Biol*. 55(3-4):395-403.
21. Stander A, Joubert F, Joubert A. (2011) Docking, synthesis, and in vitro evaluation of antimitotic estrone analogs. *Chem Biol Drug Des*. 77(3):173-181.
22. Visagie MH, Joubert AM. (2010) The in vitro effects of 2-methoxyestradiol-bis-sulphamate on cell numbers, membrane integrity and cell morphology, and the possible induction of apoptosis and autophagy in a non-tumorigenic breast epithelial cell line. *Cell Mol Biol Lett*. 15(4):564-581.
23. Newman SP, Foster PA, Ho YT, Day JM, Raobaikady B, Kasprzyk PG, et al. (2007) The therapeutic potential of a series of orally bioavailable anti-angiogenic microtubule disruptors as therapy for hormone-independent prostate and breast cancers. *Br J Cancer*. 97(12):1673-1682.
24. Foster PA, Ho YT, Newman SP, Kasprzyk PG, Leese MP, Potter BV, et al. (2008) 2-MeOE2bisMATE and 2-EtE2bisMATE induce cell cycle arrest and apoptosis in breast cancer xenografts as shown by a novel ex vivo technique. *Breast Cancer Res Treat*. 111(2):251-260.
25. Parsons MF, Foster PA, Chander SK, Jhalli R, Newman SP, Leese MP, et al. (2008) The in vivo properties of STX243: a potent angiogenesis inhibitor in breast cancer. *Br J Cancer*. 99(9):1433-1441.
26. Chander SK, Foster PA, Leese MP, Newman SP, Potter BV, Purohit A, et al. (2007) In vivo inhibition of angiogenesis by sulphamoylated derivatives of 2-methoxyoestradiol. *Br J Cancer*. 96(9):1368-1376.
27. Leese MP, Leblond B, Smith A, Newman SP, Di Fiore A, De Simone G, et al. (2006) 2-substituted estradiol bis-sulfamates, multitargeted antitumor agents: synthesis, in vitro SAR, protein crystallography, and in vivo activity. *J Med Chem*. 49(26):7683-7696.
28. Ho YT, Purohit A, Vicker N, Newman SP, Robinson JJ, Leese MP, et al. (2003) Inhibition of carbonic anhydrase II by steroidal and non-steroidal sulphamates. *Biochem Biophys Res Commun*. 305(4):909-914.
29. Supuran CT, Scozzafava A. (2007) Carbonic anhydrases as targets for medicinal chemistry. *Bioorg Med Chem*. 15(13):4336-4350.
30. Pastorekova S, Ratcliffe PJ, Pastorek J. (2008) Molecular mechanisms of carbonic anhydrase IX-mediated pH regulation under hypoxia. *BJU Int*. 101 Suppl 4:8-15.
31. Leese MP, Hejaz HA, Mahon MF, Newman SP, Purohit A, Reed MJ, et al. (2005) A-ring-substituted estrogen-3-O-sulfamates: potent multitargeted anticancer agents. *J Med Chem*. 48(16):5243-5256.
32. Chen JL, Merl D, Peterson CW, Wu J, Liu PY, Yin H, et al. Lactic acidosis triggers starvation response with paradoxical induction of TXNIP through MondoA. *PLoS Genet*. 6(9)
33. Knoechel TR, Tucker AD, Robinson CM, Phillips C, Taylor W, Bungay PJ, et al. (2006) Regulatory roles of the N-terminal domain based on crystal structures of human pyruvate dehydrogenase kinase 2 containing physiological and synthetic ligands. *Biochemistry*. 45(2):402-415.
34. Garber K. (2006) Energy deregulation: licensing tumors to grow. *Science*. 312(5777):1158-1159.

35. Ristow M. (2006) Oxidative metabolism in cancer growth. *Curr Opin Clin Nutr Metab Care*. 9(4):339-345.
36. Schulz TJ, Thierbach R, Voigt A, Drewes G, Mietzner B, Steinberg P, et al. (2006) Induction of oxidative metabolism by mitochondrial frataxin inhibits cancer growth: Otto Warburg revisited. *J Biol Chem*. 281(2):977-981.
37. Xiao L, Li X, Niu N, Qian J, Xie G, Wang Y. (2010) Dichloroacetate (DCA) enhances tumor cell death in combination with oncolytic adenovirus armed with MDA-7/IL-24. *Mol Cell Biochem*.
38. Liu H, Hu YP, Savaraj N, Priebe W, Lampidis TJ. (2001) Hypersensitization of tumor cells to glycolytic inhibitors. *Biochemistry*. 40(18):5542-5547.
39. Tagg SL, Foster PA, Leese MP, Potter BV, Reed MJ, Purohit A, et al. (2008) 2-Methoxyoestradiol-3,17-O,O-bis-sulphamate and 2-deoxy-D-glucose in combination: a potential treatment for breast and prostate cancer. *Br J Cancer*. 99(11):1842-1848.
40. Xing JZ, Zhu L, Jackson JA, Gabos S, Sun XJ, Wang XB, et al. (2005) Dynamic monitoring of cytotoxicity on microelectronic sensors. *Chem Res Toxicol*. 18(2):154-161.
41. Kirstein SL, Atienza JM, Xi B, Zhu J, Yu N, Wang X, et al. (2006) Live cell quality control and utility of real-time cell electronic sensing for assay development. *Assay Drug Dev Technol*. 4(5):545-553.
42. Sun RC, Fadia M, Dahlstrom JE, Parish CR, Board PG, Blackburn AC. (2009) Reversal of the glycolytic phenotype by dichloroacetate inhibits metastatic breast cancer cell growth in vitro and in vivo. *Breast Cancer Res Treat*.
43. Wong JY, Huggins GS, Debidda M, Munshi NC, De Vivo I. (2008) Dichloroacetate induces apoptosis in endometrial cancer cells. *Gynecol Oncol*. 109(3):394-402.
44. Gillies RJ, Didier N, Denton M. (1986) Determination of cell number in monolayer cultures. *Anal Biochem*. 159(1):109-113.
45. Kueng W, Silber E, Eppenberger U. (1989) Quantification of cells cultured on 96-well plates. *Anal Biochem*. 182(1):16-19.
46. Grever MR, Schepartz SA, Chabner BA. (1992) The National Cancer Institute: cancer drug discovery and development program. *Semin Oncol*. 19(6):622-638.
47. Joubert A, Marais S, Maritz C. (2009) Influence of 2-methoxyestradiol on MCF-7 cells: an improved differential interference contrasting technique and Bcl-2 and Bax protein expression levels. *Biocell*. 33(1):67-70.
48. Danz R, Vogelgsang A, Käthner R. PlasDIC - a useful modification of the differential interference contrast according to Smith/Nomarski in transmitted light arrangement Carl Zeiss Inc., Germany; 2004; Available from: http://www.zeiss.com/C12567BE00472A5C/EmbedTitelIntern/Article-PlasDic_Photonic_e/$File/PlasDIC_Photonik_2004March_e.pdf.
49. Klionsky DJ, Cuervo AM, Seglen PO. (2007) Methods for monitoring autophagy from yeast to human. *Autophagy*. 3(3):181-206.
50. Martin SJ, Reutelingsperger CP, McGahon AJ, Rader JA, van Schie RC, LaFace DM, et al. (1995) Early redistribution of plasma membrane phosphatidylserine is a general feature of apoptosis regardless of the initiating stimulus: inhibition by overexpression of Bcl-2 and Abl. *J Exp Med*. 182(5):1545-1556.
51. Olszewski U, Poulsen TT, Ulsperger E, Poulsen HK, Geissler K, Hamilton G. (2010) In vitro cytotoxicity of combinations of dichloroacetate with anticancer platinum compounds. *Clinical Pharmacology: Advances and Applications*. 2:177 - 183.
52. Fiebiger W, Olszewski U, Ulsperger E, Geissler K, Hamilton G. (2011) In vitro cytotoxicity of novel platinum-based drugs and dichloroacetate against lung carcinoid cell lines. *Clinical & translational oncology*. 13(1):43-49.

53. Dhar S, Lippard SJ. (2009) Mitaplatin, a potent fusion of cisplatin and the orphan drug dichloroacetate. *Proc Natl Acad Sci U S A*. 106(52):22199-22204.
54. Fukui M, Zhu BT. (2009) Mechanism of 2-methoxyestradiol-induced apoptosis and growth arrest in human breast cancer cells. *Mol Carcinog*. 48(1):66-78.
55. Mazurek S, Michel A, Eigenbrodt E. (1997) Effect of extracellular AMP on cell proliferation and metabolism of breast cancer cell lines with high and low glycolytic rates. *J Biol Chem*. 272(8):4941-4952.
56. Bonnet S, Archer SL, Allalunis-Turner J, Haromy A, Beaulieu C, Thompson R, et al. (2007) A mitochondria-K^+ channel axis is suppressed in cancer and its normalization promotes apoptosis and inhibits cancer growth. *Cancer Cell*. 11(1):37-51.
57. Scherz-Shouval R, Elazar Z. Regulation of autophagy by ROS: physiology and pathology. *Trends Biochem Sci*. 36(1):30-38.